STABILITY ANALYSIS IN BOUNDARY LAYER BEHIND A ROUGHNESS WITH FREE-STREAM TURBULENCE

Tristan M. Römer
Institute of Aerodynamics and Gas Dynamics
University of Stuttgart
Pfaffenwaldring 21, D-70569 Stuttgart, Germany
roemer@iag.uni-stuttgart.de

Ulrich Rist
Institute of Aerodynamics and Gas Dynamics
University of Stuttgart
Pfaffenwaldring 21, D-70569 Stuttgart, Germany
rist@iag.uni-stuttgart.de

ABSTRACT

An investigation of laminar-turbulent transition behind a cylindrical roughness element in the boundary layer with controlled free-stream turbulence (FST) is performed using hot-film measurements. Different levels of FST are generated by a bubble generator and a grid. An equation for determining the transition Reynolds number as a function of FST is presented. FST is higher at the leading edge of the plate with grid, but decays much faster in the streamwise direction. It is suggested that the boundary layer with roughness is not mainly receptive to FST at the leading edge of the flat plate, but rather at the cylinder and in its wake.

The results of a measurement campaign in the wake of the cylinder shows that FST lowers the entire instability range to lower Reynolds number, explaining the lower transition Reynolds number at higher FST. A power spectral density (PSD) analysis reveals that the shedding frequency of hairpin vortices is independent of FST. However, the hairpin development starts and decays at lower Reynolds numbers with FST. Above a certain FST level (here $Tu = 1.95\,\%$), the hairpin development becomes too unstable and hairpins decay immediately after their initial generation, should they develop at all.

INTRODUCTION

Precise prediction of laminar-turbulent transition in boundary layers under given conditions could improve the design of an airfoil with respect to drag. However, the prediction of transition is not straightforward, since it depends on disturbances like roughness and free-stream turbulence (FST). The experimental results of roughness-induced transition with various aspect ratios of the roughness elements from different authors is summarized by von Doenhoff & Braslow (1961). It was found that despite the same measurement setup, there is a variation in laminar-turbulent transition between the authors. This could be attributed to the varying measuring systems, which have slightly different levels of FST. Fransson & Shahinfar (2020) presented a transition semi-empirical prediction model that determines the transition as a function of the FST level Tu and the integral length scale. Whereas these authors focused on FST without roughness elements, Kumar *et al.* (2015) investigated the combined influence of FST and roughness elements on transition. By placing a grid at a specific streamwise wall-normal position, transition can be delayed. A numerical focus on the combination of FST and roughness elements is done by Bucci *et al.* (2021). They were able to derive predictions on instabilities that would occur as a function of the two variables. Their maximum investigated FST is $Tu = u_{rms}/U_e = 0.18\%$, with u_{rms} being the root-mean-square (*rms*) of velocity fluctuation and U_e the mean velocity of the free-stream. An experimental contribution to the roughness-induced transition with higher FST as in Bucci *et al.* (2021) is provided by Puckert *et al.* (2021). These authors determined the transition Reynolds number $Re_{k,tr}$ for two higher levels of FST. Re_k is defined by U_e and k, with k being the height of the roughness element. However, the influence of FST in the streamwise direction is not considered, which - as will be shown in this paper - has an effect on transition. Therefore, the experimental setup used in Puckert *et al.* (2021) is revisited and extended to include detailed measurements with respect to an extended FST range by two different types of turbulence generators. Instead of a grid with vertical bars, a crossed grid is used here to minimize the wall-normal turbulence variation. The following questions will be answered:

- Which influence does a decreasing FST have on $Re_{k,tr}$ compared to an almost constant FST in streamwise direction?
- How does $Re_{k,tr}$ depend on Tu with constant FST in the streamwise direction?
- How is the hairpin vortex development affected by FST?

Test Facility

Experiments have been performed in the laminar-water-channel (Laminar-Wasser-Kanal, LaWaKa) at the Institute of Aerodynamics and Gas Dynamics (IAG) at the University of Stuttgart. The LaWaKa is a closed-loop water facility that provides a reproducible measurement environment for flat plate laminar boundary layer studies. It has a turbulence intensity of $Tu = 0.05\,\%$ between $0.1 - 10\,\text{Hz}$ (Wiegand, 1996). A steady two-dimensional (2D) laminar boundary layer forms on the flat plate, where the leading edge has an elliptical nose. Wiegand (1996) showed that there is a high agreement between the theoretical and measured flow in the LaWaKa.

The measurements are carried out using a Dantec 55R15 hot-film probe, whose position can be set by a traverse system. A Dantec Streamware bridge is connected with the hot-film probe and works according to the constant temperature anemometry principle. The output voltage of the bridge is recorded with a 16-bit National Instruments USB-6216 A/D converter and converted to velocity u through King's law.

Experimental Setup

A cylindrical roughness element with height $k = 0.01\,\mathrm{m}$ and width $d = k$ (aspect ratio $\eta = d/k = 1$) is placed 0.57 m behind the leading edge in the center of the flat plate. The coordinate x represents the distance from the leading edge and y the wall-normal position. Unless otherwise noted, the coordinates x,y and z are nondimensionalized with respect to k. According to this notation, the roughness element is placed at $x = (0.57\,\mathrm{m})/k = (0.57\,\mathrm{m})/(0.01\,\mathrm{m}) = 57$.

To generate controlled FST, two different turbulence generators have been developed: a bubble generator and a coarse grid. The bubble generator allows a continuous adjustment of the FST level by modification of the release rate of rising air bubbles from a strip upstream of the leading edge. A fine grid is placed between the bubble generator and the leading edge to allow for better control of the turbulence level and enable a homogeneous spanwise turbulence distribution. Three different pressures $p = 0.1\,\mathrm{bar}$, $p = 0.2\,\mathrm{bar}$ and $p = 0.3\,\mathrm{bar}$ are considered, named setup B_1, B_2 and B_3, respectively. The second mechanism is based on a welded grid, with cylindrical wires forming a lattice with square holes (setup G). The mesh width is $M = 25\,\mathrm{mm}$ having wire diameter $g = 1.6\,\mathrm{mm}$. The grid dimensions have been chosen such that $Re_g = U_e g/\nu > 40$. This requirement was determined by Roach (1987). It indicates that vortex shedding is present, leading to an increase of FST. A lower Re_g value would lead to a reduction of FST, as shown by e.g. Puckert *et al.* (2017). Moreover, the porosity

$$\beta = \left(1 - \frac{g}{M}\right)^2 = 0.876 \qquad (1)$$

should be larger than 0.55 to avoid large-scale mean velocity variations, as pointed out by Kurian & Fransson (2009). In order to compare the results, a reference setup R without turbulence generator is also considered. Only the fine grid is used to reduce FST at low velocities as pointed out by Puckert *et al.* (2017). Either the fine grid (setup $B_{1,2,3}$, R) or the coarse grid (setup G) is used and placed at $x = -25$. The complete measurement setup with both turbulence generators is illustrated in Figure 1. The various investigated setups and their parameters are summarized in Table 1.

RESULTS
Free-Stream Turbulence

A major challenge of understanding the influence of FST on transition is that an exact value of FST level along the streamwise direction x can not be adjusted in experiments. This is explained by the fact that turbulence decays without external input. Figure 2 shows the variation of Tu at several x positions for $U_e \approx 0.07\,\mathrm{m/s}$ in the free-stream. The wall-normal position is $y = 7$, which is higher than the theoretical laminar

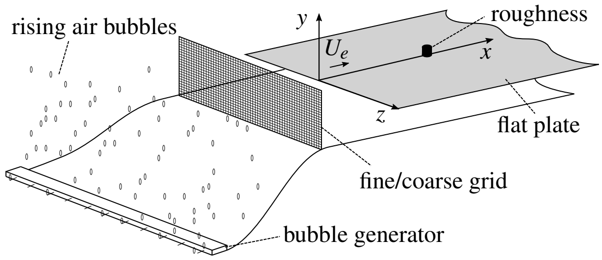

Figure 1. Test facility with experimental setup.

Table 1. Overview of setups and their parameters.

setup name		bubble generator (pressure)	fine grid	coarse grid $M = 25\,\mathrm{mm}$ $g = 1.6\,\mathrm{mm}$
R	reference		×	
B_1	bubbles	× (0.1 bar)	×	
B_2	bubbles	× (0.2 bar)	×	
B_3	bubbles	× (0.3 bar)	×	
G	grid			×

boundary layer thickness $\delta_{99}(x_{max} = 236) = 2.9$. Each data point has a measurement time duration of $t = 300\,\mathrm{s}$ and sampling rate of $f_s = 200\,\mathrm{Hz}$. The data are only band-pass filtered by the Nyquist frequency condition, i.e. $2/t = 0.0067\,\mathrm{Hz}$ and $f_s/2 = 100\,\mathrm{Hz}$. As expected, setup R shows very low Tu levels along x. Therefore, setup R will be considered a reference case with effectively no FST.

It can be seen from the grid-generated turbulence that the turbulence level decays in the streamwise direction. Tennekes & Lumley (1972) predict that the turbulent energy decays as x^{-1}, implying that the turbulence level Tu decays proportional to $x^{-1/2}$. Note that different values are given for the exponent in literature (Batchelor & Townsend, 1948; Pope, 2000; Tennekes & Lumley, 1972). For grid-generated turbulence, the decay can be fitted according to Batchelor & Townsend (1948):

$$Tu = \sqrt{A\left(\frac{x_g - x_{g,0}}{M}\right)^b} \qquad (2)$$

where x_g is the distance downstream of the grid, $x_{g,0}$ is a virtual origin, A is an individual grid constant and b is the decay rate. As shown by Kurian & Fransson (2009), the virtual origin can be set to $x_{g,0} = 0$. For setup G, the nonlinear least-square fit gives $A = 0.0153$ and $b = -1.45$. Equation (2) fits well for setup G, as can be seen in Figure 2 (dashed curve G fit).

In contrast to the grid-generated FST, the bubble-generated FST follows a relatively constant Tu-level in x-direction. This is remarkable given that no energy is input and thus a decay of the turbulence is expected. The rising air-bubbles not only cause a velocity fluctuation in the streamwise direction, but also a lateral fluctuation due to lateral quivering of the bubbles. Downstream, the lateral velocity fluctuation contributes to the spanwise fluctuation velocity. This phenomenon has also been reported by e.g. Kurian & Fransson (2009). Figure 2 also shows the proportional relationship between air-pressure and the FST, namely that higher bubble generator pressure yields a higher FST. Accordingly, the bubble setups can be ranked from low to high Tu as follows: $B_1 < B_2 < B_3$. Setup G generates the most dominant FST at $x = 0$. Downstream of $x \approx 34$, this setup has a lower FST compared to $B_{1,2,3}$. This difference will be interesting for the laminar-turbulent transition, which is discussed in the next section. In summary, the setups R and $B_{1,2,3}$ exhibit a relatively constant Tu along x, whereas setup G shows a strong decay of Tu in x.

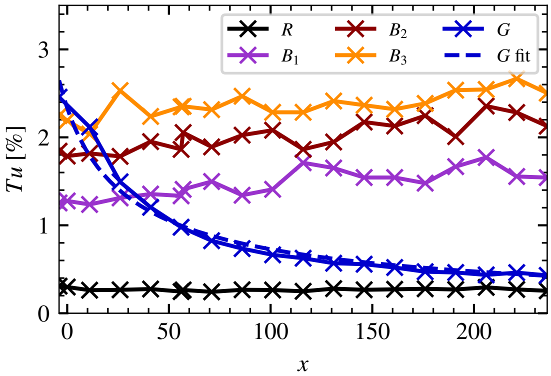

Figure 2. FST in streamwise direction at $y = 7$, $z = 0$.

Laminar-Turbulent Transition

To determine the transition Reynolds number $Re_{k,tr}$, measurements are carried out at the fixed position $x = 157, y = 1$ with increasing Re_k by varying U_e. Each measurement has a duration of 600 s and sampling rate of 200 Hz. The measurements are then evaluated by the intermittency function γ as described by Zhang *et al.* (2013), where γ varies between 0 and 1. If $\gamma = 0$, the underlying flow is laminar, whereas $\gamma = 1$ would indicate turbulent flow. The transition region lies between $0.1 < \gamma < 0.9$. In this region, $Re_{k,tr}$ is defined where $\gamma = 0.5$. Here, a slight modification compared to Zhang *et al.* (2013) is performed. The velocity signal is band-pass filtered between $0.5 - 10$ Hz before evaluating the intermittency, which is similar to the procedure from Fransson *et al.* (2005). In Figure 3, the top line shows the unfiltered velocity signal and the bottom line represents the band-pass filtered velocity signal from setup G for $Re_k = 626$. Figure 3 makes clear that turbulent spots can be recorded, but mean velocity deviation and signal noise are filtered out. This allows for the more accurate derivation of the intermittency function. After evaluating the intermittency, the values are least-square fitted to:

$$\gamma(Re_k) = \frac{1}{1 + e^{-c_1(Re_k - c_2)}} \tag{3}$$

where c_1 and c_2 are constants.

Figure 4 shows the intermittency functions for all setups. In general, the resulting Re_k range for $0.1 < \gamma < 0.9$ is wider with FST and matches the experiments from Puckert *et al.* (2021). This can be explained by the fact that, due to higher FST, there is more turbulent energy in the free-stream. Disturbances at the roughness element are amplified by the free-stream/boundary layer receptivity and have a higher amplitude with FST than without FST. Details are provided in the next section. However, the general assumption that the transition region increases with higher FST cannot be concluded only by investigating the FST. The integral length scale has an additional influence on the transition range, as also found without roughness by Fransson & Shahinfar (2020). From the present observations, the integral length scale must play a key role in the transition region and should be investigated in more detail. The focus of this paper is on the influence of FST.

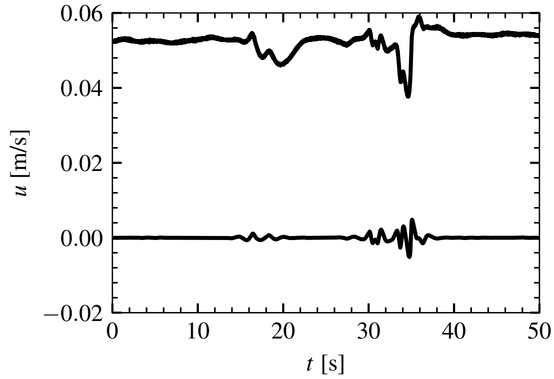

Figure 3. Unfiltered (top) and filtered velocity (bottom) measured with setup G at $Re_k = 626$, $0\,\mathrm{s} \leq t \leq 50\,\mathrm{s} < t_{max} = 600\,\mathrm{s}$ and $x = 157, y = 1, z = 0$.

The R setup has the transition Reynolds number $Re_{k,tr} = 670$. With setup G, the transition Reynolds number is reduced to $Re_{k,tr} = 654$. The bubble-generated FST setups B_1, B_2 and B_3 reduce the transition Reynolds number to $Re_{k,tr} = 616$, $Re_{k,tr} = 575$ and $Re_{k,tr} = 549$, respectively. Although setup B_1 has a lower FST level than setup G at $x = 0$ (compare Figure 2), the transition Reynolds number is by far lower. This is astonishing at first, because it is known that $Re_{k,tr}$ decreases as Tu increases. The reason for this can be attributed to the higher turbulence level of setup $B_{1,2,3}$ downstream of the roughness. Thus, the first question of this paper can be addressed. From the presently investigated FST levels, the roughness-induced boundary layer is mainly receptive to FST at and downstream of the roughness element rather than to FST upstream of the roughness element.

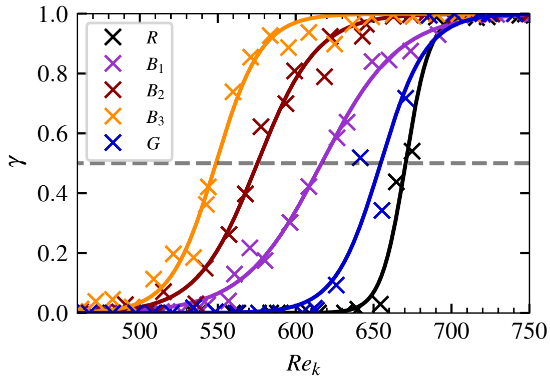

Figure 4. Evaluated intermittency function.

Given $Re_{k,tr}$ for the various setups, a correlation between $Re_{k,tr}$ and Tu can be determined, i.e. $Re_{k,tr}(Tu)$. This requires to assign $Re_{k,tr}$ of each setup to one Tu level. For the bubble generator $B_{1,2,3}$ and the reference R setups, Tu is relatively constant in the streamwise direction. Therefore, for these setups the Tu averages along x are calculated from Figure 2. The values $Tu = 0.27\,\%$ (R), $Tu = 1.43\,\%$ (B_1), $Tu = 1.95\,\%$ (B_2) and $Tu = 2.32\,\%$ (B_3) are assigned to their corresponding $Re_{k,tr}$ from Figure 4 and depicted as a cross in Figure 5. Note that the average is calculated for the range $0 \leq x \leq 161$, so that all measuring points from the intermittency measurement (Figure 4) are included, but the insignificant FST upstream of the leading edge is not taken into account. With setup $B_{1,2,3}$ and R (constant FST setups) the linear fit

$$Re_{k,tr}(Tu) = 690 - 58.7 \cdot 10^2 Tu \qquad (4)$$

is calculated and is shown as a solid gray line in Figure 5. The linear Equation (4) fits well and can be used to calculate $Re_{k,tr}$ by a given Tu. It should be emphasized that Equation (4) assumes a constant Tu in the streamwise direction. It is not straightforward to determine a specific Tu for setup G, since the FST decays rapidly in the streamwise direction. This can be comprehended by the error-bars in Figure 5, which indicate the minimum and maximum Tu from Figure 2 in the range $0 \leq x \leq 161$ for all setups. The minimum and maximum Tu for setups $B_{1,2,3}$ and R (solid lines) are closer together than in setup G (dashed line), since they follow a relatively constant FST level along x. For setup G, the minimum Tu is located at $x = 161$ and the maximum at $x = 0$, as shown in Figure 2. An analogous Tu is calculated for setup G based on the linear trend shown in Equation (4) and Figure 5. Given $Re_{k,tr} = 650$ for setup G, the equivalent Tu can be found to be $0.61\,\%$. This means that setup G acts like a bubble-generator, which causes a FST of $Tu = 0.61\,\%$. Or, to be more general, setup G acts like a constant FST environment with $Tu = 0.61\,\%$.

For comparison, the gray background in Figure 5 shows the lower and higher range of the von Doenhoff & Braslow (1961) transition diagram for $\eta = 1$. The range marks where $Re_{k,tr}$ was found for different roughness element experiments in the literature without additional FST. If Re_k of an experiment is below the gray range, the flow downstream of the roughness remains laminar. Above the range, the flow has already passed transition. Note that the original von Doenhoff & Braslow diagram only displays $Re_{k,tr}$ points. The range in Figure 5 is derived from Bucci *et al.* (2021). All presently investigated setups lie within this range. Setup R is clearly below the upper limit, although the FST is very low. This reveals that there is another influencing factor which explains the varying $Re_{k,tr}$ in the von Doenhoff & Braslow diagram. One such factor is that experiments are included in the diagram with more than one cylinder. Moreover, different facilities lead to a deviating base-flow. More detailed explanations have been reported by e.g. Bucci *et al.* (2021). Setup B_3 with $Tu = 2.32\,\%$ is located at the lower limit. This indicates that constant FST levels higher than $Tu > 2.32\,\%$ were not present in experiments summarized by von Doenhoff & Braslow (1961).

Velocity Fluctuation Analysis

A velocity fluctuation analysis with setups $R_{1,2,3}$ is performed, which focuses on constant FST along x. Comparison is enabled by reference setup R. Measurements are taken in the center of the plate downstream of the roughness element at fixed position $y = 1$ and $z = 0$ at evenly spaced intervals of $\Delta x = 2$ from $x = 59$ to $x = 109$. The interval lies between the roughness element ($x = 57$) and the intermittency measurement from Figure 4 ($x = 157$). At each measurement position, the free-stream velocity was uniformly increased to obtain 29 equally distributed Re_k in ascending order. One measurement

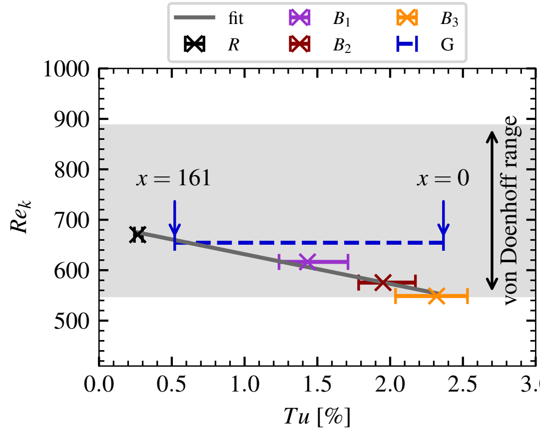

Figure 5. $Re_{k,tr}$ for all setups and corresponding average Tu (marked as a cross, only setup $B_{1,2,3}$, R) from Figure 2. The error bars show the minimum and maximum Tu level between $0 \leq x \leq 161$. Gray background indicates lower and higher limit of $Re_{k,tr}$ according to von Doenhoff & Braslow (1961).

series results in 754 discrete measurements, where each discrete measurement has a duration of 60 s and a sampling rate of 100 Hz. This results in a total measurement duration of 50.27 hours. Band-pass filtering is applied between 0.1 and 10 Hz.

Figure 6 illustrates the distribution of u'_{rms}/U_e as a function of Re_k and x. In the region $Re_k < 570$, no fluctuations are present for setup R. This region can be interpreted as steady or quasi-steady (Puckert, 2019). Such a steady region can not be clearly identified with FST. However, looking at the various setups at $Re_k < 670$, it appears that the entire lower fluctuation range moves to lower Re_k as FST increases. To get a better understanding of this phenomenon, Figure 7 illustrates the lower fluctuation range ($u'_{rms}/U_e = 0.03$) for setups R, B_1 and B_3 by dashed lines. For clarity, setup B_2 is not shown, although the conclusions drawn are equivalent. Thus, with an increase of FST, disturbances are more amplified at lower Re_k, which leads to an unstable boundary layer at lower Re_k. This explains why an increase of Tu results in a decrease of $Re_{k,tr}$. Setup B_1 has a less steady contour along x compared to R, and the contour for B_3 is even less constant. Hence, it is clear that FST leads not only to a lower $Re_{k,tr}$, but also to a larger transition range along Re_k (compare Figure 4).

For $60 < x < 70$ at $Re_k > 550$, the most dominant fluctuations appear for all setups. This region is marked by solid lines in Figure 7, where $u'_{rms}/U_e = 0.09$. Note that only $59 \leq x \leq 73$ is plotted for the solid lines. Such a region can be associated with the development of hairpin vortices (Puckert, 2019). Hairpin vortices periodically shed downstream of the roughness element, if a certain Re_k is exceeded (Loiseau *et al.*, 2014). As outlined in Puckert (2019) without FST, an increase of Re_k has almost no effect on the upstream front of this region, which settles here at $x = 61$ for $u'_{rms}/U_e = 0.09$. However, with FST the front moves towards the roughness element ($x = 60$). This effect can be explained by the higher ambient fluctuation. The disturbances require a shorter distance to become amplified to the same amplitude level of lower FST. An increase in FST also stretches this region to lower Re_k, indicating that hairpins start to develop at lower Re_k.

To get insights into the FST influence on the development of hairpins, the power spectral density (PSD) of u' is plotted in Figure 8 at $x = 63$, which lies in the hairpin development region (compare to Figure 7). Note that similar results are ob-

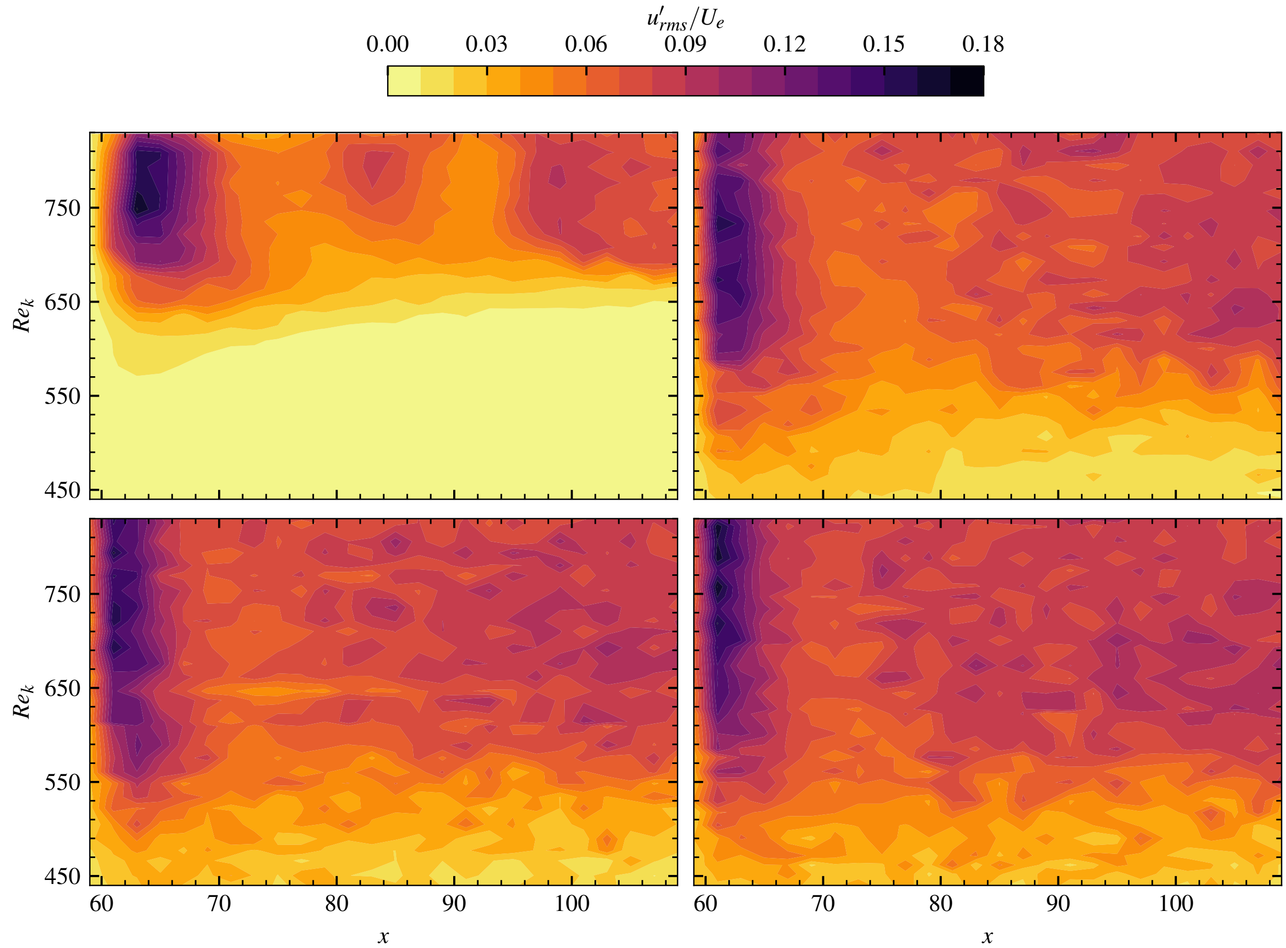

Figure 6. Contour plots of u'_{rms}/U_e. Top left: R, top right: B_1, bottom left: B_2, bottom right B_3.

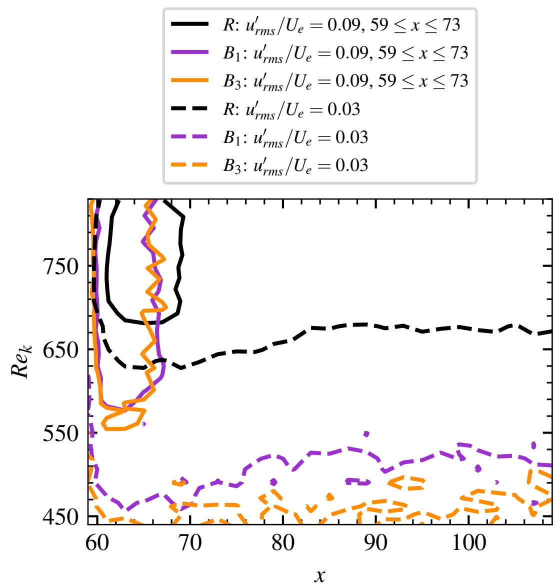

Figure 7. Specific u'_{rms}/U_e values for R, B_1 and B_3.

tained in the area $62 < x < 66$. The non-dimensional angular frequency $\omega = 2\pi f k/U_e$ is calculated with the physical frequency f in Hz. In the reference setup R, a clear harmonic structure starting at $Re_k = 650$ can be observed. The fundamental frequency is $\omega \approx 1$ and grows slightly with Re_k. Puckert (2019) has shown that the harmonic can be associated with hairpin vortex shedding. Looking at the dashed line in Figure 8, the slope and ω-intercept of the harmonic structure along Re_k is not affected by FST. Thus, the shedding frequency of the hairpin vortices behind the roughness element is independent of FST. However, three differences to the reference setup R can be determined. First, the harmonic structure starts at a lower Re_k with FST. Second, as FST increases, the maximum PSD tends to decrease and become noisier outside the fundamental frequency. Third, a higher harmonic structure in the range $\omega \approx 2$, $Re_k > 690$ can be identified only for R. From the observations, the following statements can be implied for the hairpin vortex development:

- The hairpin vortex both develops and collapses with FST at lower Re_k.
- Above a certain FST the hairpin, if present at all, collapses immediately.

The FST of the second statement is here set to $Tu = 1.95\,\%$ (setup B_2), which is chosen visually by Figure 8 and should therefore be regarded as an estimate. Accordingly, bypass transition may be present in B_2 and B_3, but not in B_1 and R. The two results clarify why in Figure 7 the solid lines ($u'_{rms}/U_e = 0.09$) tend to be more elongated along Re_k and more narrow-banded in x compared to R.

CONCLUSION

The influence of FST on stability behind a roughness element has been investigated by two types of FST genera-

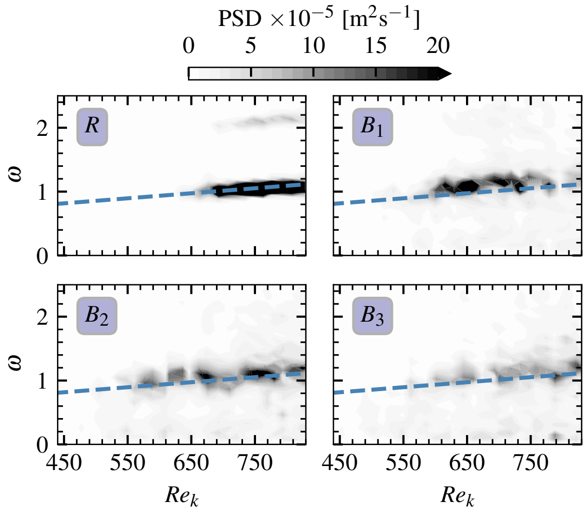

Figure 8. Spectral analysis by PSD at $x = 63$, $y = 1$, $z = 0$. The dashed line is displayed for comparison.

tors: a bubble generator and a coarse grid. From the studies conducted here, the general hypothesis can be confirmed that $Re_{k,tr}$ is reciprocal proportional to Tu. As shown by the grid-generated FST, a strong decay of Tu is usually present in various experiments in the literature and it is therefore not straightforward to assign $Re_{k,tr}$ to a specific Tu. With the given equation, Re_k can now be determined as a function of Tu, assuming that Tu is relatively constant in streamwise direction. This has been made possible by the bubble-generator experiments, where Tu varies only slightly in the investigated streamwise range. From the results it is suggested that the boundary layer with a roughness element is receptive to FST at or downstream of the element rather than upstream. However, further measurements with other grids are needed to reinforce this statement.

The investigation of the fluctuation power behind the roughness element has shown that disturbances are more amplified at lower Re_k with increased FST. The entire lower fluctuation range is moved to lower Re_k and is more unsteady along x, explaining the larger transition range along Re_k and lower $Re_{k,tr}$. In addition, a PSD analysis shows that the shedding frequency of the hairpin vortices ($\omega \approx 1$) is independent of FST. However, it is implied that hairpins develop and decay at lower Re_k. If the FST is too high, the development of hairpins is disturbed too significantly and thus they are directly broken up. Here, this limit is set to $Tu = 1.95\,\%$, but should be validated by further experiments and visualizations.

ACKNOWLEDGMENT

The funding of the Deutsche Forschungsgemeinschaft (DFG) under grant number RI 680/39-1 is acknowledged.

REFERENCES

Batchelor, G. K. & Townsend, A. A. 1948 Decay of isotropic turbulence in the initial period. *Proceedings of the Royal Society of London. Series A. Mathematical and Physical Sciences* **193** (1035), 539–558.

Bucci, M. A., Cherubini, S., Loiseau, J.-Ch., Robinet, J.-Ch., Loiseau, J.-C. & Robinet, J.-C. 2021 Influence of freestream turbulence on the flow over a wall roughness. *Physical Review Fluids* **6** (6).

von Doenhoff, A. E. & Braslow, A. L. 1961 The effect of distributed roughness on laminar flow. *Boundary Layer Control* **2**, 657–681.

Fransson, J. H. M., Matsubara, M. & Alfredsson, P. H. 2005 Transition induced by free-stream turbulence. *Journal of Fluid Mechanics* **527**, 1–25.

Fransson, J. H. M. & Shahinfar, S. 2020 On the effect of free-stream turbulence on boundary-layer transition. *Journal of Fluid Mechanics* **899**, A23.

Kumar, P. P., Mandal, A. C. & Dey, J. 2015 Effect of a mesh on boundary layer transitions induced by free-stream turbulence and an isolated roughness element. *Journal of Fluid Mechanics* **772**, 445–477.

Kurian, T. & Fransson, J. H. M. 2009 Grid-generated turbulence revisited. *Fluid Dynamics Research* **41**, 021403.

Loiseau, J.-C., Robinet, J.-C., Cherubini, S. & Leriche, E. 2014 Investigation of the roughness-induced transition: global stability analyses and direct numerical simulations. *Journal of Fluid Mechanics* **760**, 175–211.

Pope, S. B. 2000 Turbulent flows, 1st edn. Cambridge: Cambridge Univ. Press.

Puckert, D. K. 2019 Experimental investigation on global instability and critical reynolds number in roughness-induced laminar-to-turbulent transition. PhD thesis, Universität Stuttgart, Stuttgart.

Puckert, D. K., Dieterle, M. & Rist, U. 2017 Reduction of freestream turbulence at low velocities. *Experiments in Fluids* **58** (5).

Puckert, D. K., Römer, T. M., Scibelli, G. & Rist, U. 2021 Experimental investigation on roughness-induced transition under the influence of freestream turbulence. In *New Results in Numerical and Experimental Fluid Mechanics XIII* (ed. Dillmann et al.), *Notes on Numerical Fluid Mechanics and Multidisciplinary Design*, vol. 151, pp. 205–214. Cham: Springer International Publishing.

Roach, P. E. 1987 The generation of nearly isotropic turbulence by means of grids. *International Journal of Heat and Fluid Flow* **8** (2), 82–92.

Tennekes, H. & Lumley, J. L. 1972 A first course in turbulence. Cambridge, Massachusetts and London, England: MIT Press.

Wiegand, T. 1996 Experimentelle untersuchungen zum laminar-turbulenten transitionsprozeß eines wellenzuges in einer plattengrenzschicht. PhD thesis, Universität Stuttgart, Stuttgart.

Zhang, J., Xu, M., Pollard, A. & Mi, J. 2013 Effects of external intermittency and mean shear on the spectral inertial-range exponent in a turbulent square jet. *Physical review E* **87** (5), 053009.